Icarus 242 (2014) 122–129

Contents lists available at ScienceDirect

Icarus

journal homepage: www.elsevier.com/locate/icarus

The global vortex analysis of Jupiter and Saturn based on Cassini Imaging Science Subsystem

Harold Justin Trammell [a,*], Liming Li [a], Xun Jiang [a], Mark Smith [a], Sarah Hörst [b], Ashwin Vasavada [c]

[a] University of Houston, 4800 Calhoun Road, Houston, TX 77020, United States
[b] University of Colorado at Boulder, Box 216 UCB, Boulder, CO 80309-0216, United States
[c] Jet Propulsion Laboratory, M/S 264-640, 800 Oak Grove Drive, Pasadena, CA 91109, United States

ARTICLE INFO

Article history:
Received 23 October 2013
Revised 17 July 2014
Accepted 17 July 2014
Available online 4 August 2014

Keywords:
Saturn, atmosphere
Atmospheres, dynamics
Atmospheres, structure
Image processing

ABSTRACT

Presented in this manuscript are observations exploring vortices with diameters larger than 1000 km on Jupiter and Saturn. These images are taken from the Imaging Science Subsystem onboard the Cassini Spacecraft. The analyses of Saturn's vortices show that there are significantly more vortices in the Southern Hemisphere (SH) than in the Northern Hemisphere (NH) during the time from 2004 to 2010. In particular, the concentration of vortices are completely different between the two hemispheres, especially in the latitude band around 40°N where the 2010 giant storm occurred. In the SH, the latitude band around 40°S has the highest concentration of vortices on Saturn. Contrasting results show that vortices are lacking in the latitudinal band around 40°N in the NH before the eruption of the 2010 giant storm, although zonal wind characteristics are similar at both locations. Global maps of Saturn at different times suggest that the total numbers of large vortices dramatically decreased from 29 ± 1 to 11 ± 2 in the SH and from 11 ± 2 to 7 ± 1 in the NH during this time period (2004–2010), just before the eruption of the giant storm at the end of 2010. The goal here is to present observational trends and evaluate if the temporal variation in the total number of vortices is related to the eruption of the 2010 giant storm. The comparison of jovian and saturnian vortices shows that the contrast of the two hemispheres is different between the two giant planets, likely due to the different obliquities, hence different seasonal cycles on the two planets. Jovian vortices tend to display a near equal distribution of vortices across hemispheres, while saturnian vortices are distributed unevenly. The comparison also reveals that on both planets, there is a correlation between the highest number of vortices and the westward jet peaks. This suggests that atmospheric instabilities play a critical role in generating vortices on both planets.

1. Introduction

From October 1, 2000 to March 20, 2001, Cassini spent about half of an Earth year observing Jupiter en route to Saturn (e.g., Porco et al., 2003). Jupiter has a very small axial tilt (~3°) and a faint ring system, creating conditions where the vast majority of the planet is observable (i.e., sunlit and not occluded) during any given diurnal cycle. Cassini arrived at Saturn in 2004 and is expected to collect data until 2017, encompassing nearly one half of a saturnian year (~29.5 Earth years). Saturn's tilt is ~27.9° which is similar to Earth's at ~23.5°. Like Earth, the axial tilt of Saturn creates significant variations in the global distribution of solar flux. Additionally, Saturn's ring system blocks sunlight from the planet, creating shadows on the body in the hemisphere tilted away from the Sun. Therefore, significant seasonal variations in solar forcing occur between the two hemispheres of Saturn. The long-term Cassini observations, which include a seasonal transit in 2009 (northern spring equinox), will help explore the temporal variation of the atmospheric system of Saturn.

Due to the long-term observations available from Cassini, in this study we focus on the vortex activity on Saturn and compare these activities between Saturn and Jupiter. There are many vortices existing in the atmospheric systems of Jupiter and Saturn. These highly dynamic structures play important roles in the small and large scale atmospheric variations on these planets (e.g., Ingersoll et al., 2004; Vasavada and Showman, 2005; Del Genio et al., 2009). Analyzing vortices not only enriches our knowledge of the meteorology (e.g., Smith et al., 1981, 1982; Ingersoll et al., 1981; Sromovsky et al., 1983; Mac Low and Ingersoll, 1986; Morales-Juberias et al., 2002; Sánchez-Lavega et al., 2004; Li et al., 2004;

* Corresponding author address: University of Houston, 4800 Calhoun Road, Houston, TX 77020, United States.
E-mail address: hjtrammell@uh.edu (H.J. Trammell).

http://dx.doi.org/10.1016/j.icarus.2014.07.019
0019-1035/

Salyk et al., 2006; Vasavada et al., 2006; Del Genio et al., 2007), but also helps better understand the large-scale atmospheric dynamics on the two Gas Giant Planets (e.g., Ingersoll and Cuong, 1981; Williams and Yamagata, 1984; Dowling and Ingersoll, 1989; Marcus et al., 2000; Li et al., 2006a; Showman, 2007; del Rio-Gaztelurrutia et al., 2010).

The high spatial resolution images recorded by the Imaging Science Subsystem (ISS) on Cassini provide a perfect opportunity to examine saturnian vortex activities in detail over specific time frames. From the Cassini observations in 2004, Vasavada et al. (2006) studied Saturn's vortices in the Southern Hemisphere (SH). Due to the seasonal ring sunlight blockage and Cassini's orbital path, a vast majority of the Northern Hemisphere (NH) of Saturn was shaded or hidden from observation during the 2004-era observations. Additionally, some specific vortices in the SH (del Rio-Gaztelurrutia et al., 2010) and NH (Fletcher et al., 2012; Sayanagi et al., 2013) have been investigated with Cassini observations. While these studies are considered during this work, a systematic survey of Saturn's global vortices is lacking. The continuous Cassini observations make it possible to systematically investigate the vortices in the NH as well as the SH, creating a global understanding of these prevalent and robust atmospheric features.

Here, we use the public Cassini ISS observations from 2004 to 2010 to explore these oval spots over the whole globe of Saturn while emphasizing the temporal variation of these features. These oval spots are defined as vortices based on previous studies (Vasavada et al., 2006; del Rio-Gaztelurrutia et al., 2010). These studies suggested these oval spots on Saturn are characterized as vortices based on rotation and vorticity measurements. In this study, planetographic latitudes and western longitudes are utilized to define the spatial domain of these Cassini ISS processed maps. In the time domain, we use the solar longitude to track the seasonal changes on Jupiter and Saturn. Solar longitude is defined as the longitude of the Sun in the sky as seen from the planet, with 0° at the point where the Sun crosses the equator going northward (northern spring equinox). This is equivalent to the angular distance of the planet in its orbit around the Sun, creating an ideal time standard.

2. Data and data processing

The current study utilizes Cassini ISS images of Jupiter from 2000 to 2001 and of Saturn from 2004 to 2010 to conduct a global survey of vortices on the two Gas Giants. The Cassini ISS images are obtained from the archive on the public Planetary Data System (PDS). The processing of these Cassini ISS images (e.g., calibration, navigation, solar-illumination removal, and map projection) are described in detail in two previously related studies (Li et al., 2004; Vasavada et al., 2006) and are briefly summarized here.

As described in Porco et al. (2004), the Cassini ISS is equipped with 12 filters on the narrow-angle camera (NAC FOV 0.35°) and 9 on the wide-angle camera (WAC 3.5°), ranging from ultraviolet (258 nm) through near infrared (1028 nm) wavelengths (Porco et al., 2004). The filters focused on our target area are three continuum-band filters (CB1, CB2, and CB3). Data sets here are taken from the images recorded at the CB2 wavelengths (750 nm in NAC and 752 nm in WAC). The CB2 wavelength was used because the largest number of observations has been obtained in this filter and these images best reveal tropospheric cloud activities. The CB2 images predominantly detects pressure levels around 300–500 mbar (Perez-Hoyos and Sanchez-Lavega, 2006). However, it is possible that some individual features in the CB2 images can probe pressure levels down to the ammonia cloud deck (1–1.4 bar), depending on the optical thickness of the tropospheric haze (Sanchez-Lavega et al., 2007). Therefore, the CB2 images are ideal for the creation of as many complete global maps as possible. Multiple, high-quality maps are critical in the investigation of Saturn's global vortices and their temporal variations.

Data processing is conducted using several procedures. The images are first navigated by deriving the true spacecraft pointing by fitting, in the image plane, the observed planetary limb. To flatten the solar illumination, we found that a modified formula (Li et al., 2006b) based on the Minnaert function (Minnaert, 1941) works well for the ISS images of Jupiter. Ring effects complicate the solar illumination of Saturn's images. The classic Minnaert function does not work well for the ISS images of Saturn due to the scattering of light from the rings. Therefore, we use a high-pass filter as suggested by Vasavada et al. (2006) to remove the solar illumination. The processed images are then projected as cylindrical maps. After processing, each projected map occupies about 50–70° of longitude. This ideal spacing allows us to develop global maps by combining 5–7 projected images.

To obtain the highest fidelity global maps of Saturn, we selected the ISS images based on several criteria for this study. First, we selected high-quality ISS images with good spatial coverage (coverage greater than 70° of latitude) and with spatial resolution better than 200 km/pixel. The large spatial coverage and high spatial resolution are critical for the global analysis of vortices on Saturn. Second, the series of images used to produce one global map must be separated by relatively short time intervals to minimize the movement of features due to strong zonal winds, while also allowing enough rotation of Saturn to image the entire body in 5–7 images. In this study, we selected images with a time interval between the neighboring two images of less than 2.5 h. The strongest zonal winds (~400 m/s) in the equatorial region will result in a displacement of ~3600 km during a period of 2.5 h. The displacement of 3600 km corresponds to ~3.4° shift in longitudinal direction in the equatorial region of Saturn. The longitudinal shift due to the zonal winds among the series of images drops from the equator to the middle and high latitudes. This drop can be attributed to the decreased zonal winds, so the movement is further reduced, eliminating any associated issues with significant feature movement. Capturing minimal feature movements is critical in quality map development. It should be mentioned that there are longitude overlaps on the two neighboring images, which assist in achieving improved mapping accuracy. We carefully checked features in regions of longitudinal overlap to correct for possible errors of vortex counting caused by the longitude shift due to the zonal winds. The last criterion was avoiding the significant ring effects (shading and blocking in the view field). These images, with shadowing of less than 20°, are selected to process the global maps in this study.

Using these criteria, we developed two global maps of Saturn using public ISS images from 2004 to 2010, using the CB2 filter, which are summarized in Table 1. Fig. 1 shows the first CB2 global map, composed from the NH map in 2008 and the SH map in 2004. The time variation between hemispheres is due to the stringent global map development criteria, explained above. In the NH, the ring-shaded areas decrease from 2004 to 2008. During 2008, the ring-shaded latitude bands extended from the equator to ~15°N, allowing for comprehensive NH map development. The second global map (Fig. 4) was developed from images from 2010, and incurs minimal ring shadowing due to the recent equinox. Table 1 summarizes two CB2 global maps of Saturn that were recorded by ISS before and after the northern spring equinox (September 2009). Therefore, the two global maps can be used to investigate the temporal variation of vortex behavior on Saturn. Along with the two CB2 global maps of Saturn, we selected one CB2 global map of Jupiter from the global maps processed in our previous studies (Li et al., 2004, 2006b) to conduct a comparative study of vortices between Jupiter and Saturn.

Table 1
Cassini global maps processed and analyzed in this study.

Planet	Time	Solar longitude (°)	Spatial coverage	Spatial resolution (km/pixel)	Camera	Filter
Saturn	September 18, 2004	295.8	SH	~98	NAC	CB2
Saturn	February 26, 2008	341.5	NH	~94	WAC	CB2
Saturn	September 25, 2010	13.8	Global	~147	WAC	CB2
Jupiter	December 7, 2000	108.9	Global	~100	NAC	CB2

Note: The solar longitude is used to define the seasons of Jupiter and Saturn with 0°, 90°, 180°, and 270° standing for the northern spring equinox, the northern summer solstice, the northern autumn equinox, and the northern winter solstice, respectively. The resolutions shown here are the spatial resolutions of the raw ISS images, which are projected to the global maps with a map scale of 0.1°/pixel. The CB2 filter has a central wavelength of 750 nm and 752 nm for NAC and WAC, respectively.

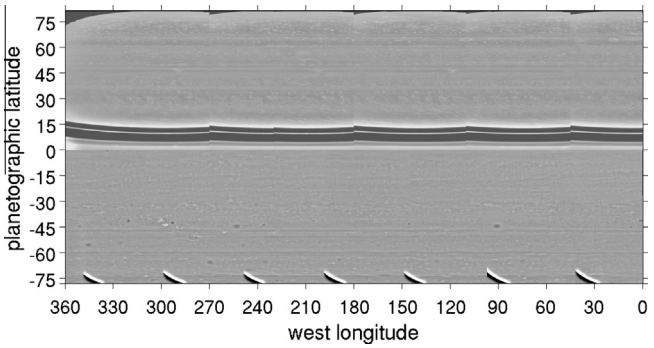

Fig. 1. First global map of Saturn observed in the CB2 filter. The global map in the NH is composed by 5 WAC images, which were observed by ISS in 2008 with a spatial resolution of ~94 km/pixel and a time separation of ~2 h. The global map in the SH is composed by 7 NAC images, which were observed by ISS in 2004 with a spatial resolution of ~98 km/pixel and a time separation of 1.5 h. These very bright and black areas in the polar region and in the northern equatorial region are the observational gaps in these images recorded by ISS.

The spatial resolution of these global maps varies from ~100 km/pixel to ~150 km/pixel (Table 1). To correctly identify the vortices, we recorded only structures that included at least ~10 pixels. Therefore, only relatively large vortices with east–west diameter larger than 1000 km are discussed here. Based on the global maps of Saturn and Jupiter, we recorded basic characteristics of these relatively large vortices including location and size. We organized these relatively large vortices into different categories by following the categories suggested in the previous study (Vasavada et al., 2006) (please also refer to Section 3.1). In regard to the sizes of the vortices, we considered the oblateness of planets (Sanchez-Lavega et al., 2007) when calculating the size of vortices in the latitude (north–south) and longitude (east–west) directions to achieve the most accurate results. We also examine the vorticity of individual vortices on Saturn. Most vortices on Jupiter are anti-cyclonic (Li et al., 2004), but the vortices on Saturn display different vorticities (Vasavada et al., 2006). Continuous global maps with short time intervals are lacking, so it is hard to measure individual vortex rotational direction and vorticity on Saturn. The previous SH study (Vasavada et al., 2006) suggests that the vorticity of each vortex is correlated to the vorticity of the local, environmental zonal winds. Here, we implement the following ideas to estimate individual vorticities: the vortices sitting in the cyclonic zones of zonal winds (i.e., vorticity of zonal winds is positive) are assumed to be cyclonic; the vortices sitting in the anti-cyclonic zones of zonal winds (i.e., vorticity of zonal winds is negative) are assumed to be anti-cyclonic. It should be mentioned that it is possible that vortices can exist in the regions of zonal winds with opposite vorticity (Li et al., 2004; Vasavada et al., 2006).

3. Results

This section summarizes the analyses of the global survey of vortices on Saturn and Jupiter. We first present the comparison between the two hemispheres of Saturn and discuss the temporal variation of Saturn's global vortices in Sections 3.1 and 3.2, respectively. Finally, the comparison of jovian and saturnian vortices is presented in Section 3.3.

3.1. Comparison of Saturn's vortices between hemispheres

Due to NH illumination limitations in the 2004 ISS observations, the previous study (Vasavada et al., 2006) discussed the vortex behavior in the SH only. Subsequent Cassini observations make it possible to explore the vortex activities in the NH. Therefore, we can conduct a global survey of the vortices on Saturn. Here, we focus on the CB2 images in the following discussions to compare Saturn's vortices between hemispheres.

To be consistent with previous SH analysis (Vasavada et al., 2006), we also divide Saturn's vortices into four categories: (1) dark; (2) dark with a bright margin; (3) bright centered; and (4) bright. There are some vortices that do not exactly match the four categories, which Vasavada et al. (2006) referred to as unclassified vortices. It is worth noting that the appearances of these unclassified vortices fall close to one of the four categories. Thus we have placed them into the closest of the four categories to simplify analysis. The numbers of vortices in the four categories are listed in Table 2. There are clear trends that can be observed out of this categorization (i.e. category 1 is dominant in the SH and category 2 and 4 are dominant in the NH). Please see Fig. 7 in Vasavada et al. (2006) for images of vortex groups.

Fig. 2 shows the ratio between the east–west diameters and the north–south diameters for the four categories of vortices. Fig. 2 suggests that the larger vortices on Saturn are more oblate. The comparison between the two hemispheres also suggests that the average ratio of the east–west diameters to the north–south diameters is larger in the SH (2.19 ± 0.29) than in the NH (1.41 ± 0.23). The values of linear-fitting ratios and the corresponding uncertainties for Fig. 2 are calculated by the least-squares method (Bevington and Robinson, 2003). Fig. 3 shows the latitudinal distri-

Table 2
Numbers of observed vortices on Saturn and Jupiter.

Planet	Spatial coverage	Time (solar longitude)	Category				Total
			1	2	3	4	
Saturn	NH	2008 (341.5°)	0	5	0	4	9
		2010 (13.8°)	0	2	0	4	6
	SH	2004 (295.8°)	16	5	5	2	28
		2010 (13.8°)	5	4	0	0	9
Jupiter	NH	2000 (108.9°)	17	6*	20	55	98
	SH	2000 (108.9°)	16	4*	32	39	91

Note: The uncertainties in the total numbers of vortices in the observational gaps are discussed in Section 3.1. The four categories of Saturn's vortices are shown in Fig. 7 of Vasavada et al. (2006), and the four categories of Jupiter's vortices are shown here in Fig. 8. It should be mentioned that the category 2 of Jupiter's vortices, which are marked with asterisks in this table, is different from the category 2 of Saturn's vortices.

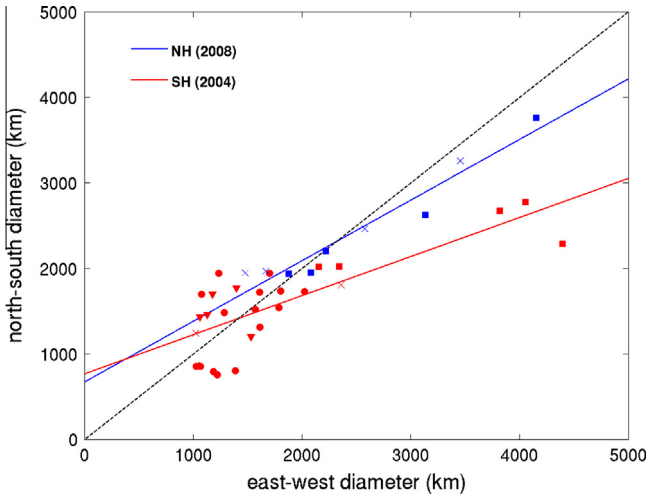

Fig. 2. Scatter plot of vortices in the two hemispheres of Saturn from 2004/2008. Circles, squares, triangles, and crosses represent category 1, 2, 3, and 4, respectively. The blue line and red line are the fitting lines for the ratios of the east–west diameters to the north–south diameters of the vortices in the NH and in the SH, respectively. The dashed black line represents the ratio as 1.0 (the east–west diameters are equal to the north–south diameters). (For interpretation of the references to color in this figure legend, the reader is referred to the web version of this article.)

bution of vortices with east–west diameters, plus the zonal wind profile from García-Melendo et al. (2011). Panel A shows that most of the vortices are concentrated in the middle and high latitudes in the two hemispheres. Panel A also displays that the category 2 vortices (dark with the bright margin) are the largest and mostly concentrated in the middle latitudes of the two hemispheres. Panel B of Fig. 3 suggests that most of the vortices in the NH are near the peak of westward zonal jets, a phenomenon previously observed in the SH (Vasavada et al., 2006). The instability of these jets around zonal wind minima (Dowling and Ingersoll, 1989; Li et al., 2004; Vasavada et al., 2006) facilitates the generation of eddies and vortices, and likely contributes to the observed distribution of vortices. The comparison between the two hemispheres in Fig. 3 further suggests a significant difference of vortex concentration around latitude 40° between the two hemispheres, even though the latitude band around 40° corresponds to the minima of zonal winds in both hemispheres. In the SH, the latitude band around 40°S has the largest number of vortices, but there is no observed vortex around the 40°N latitude band in the NH (please refer to Figs. 3 and 6 and the corresponding discussions).

Table 2 also shows that there are 28 vortices in the SH (2004), compared to only 9 large vortices in the NH (2008). When comparing the total numbers of vortices between the two hemispheres, the observational gaps (areas suffering from ring effects and observational gaps) in the two hemispheres (Fig. 1) should be considered. Here, the ratio of the area of the observational gaps to the total area is used to estimate the uncertainty in the total number of vortices in each hemisphere. The global surface area of an oblate planet (Coxeter, 1989) is calculated with

$$S = 2\pi a^2[1 + (1 - e^2)\tanh^{-1}e/e] \quad (1)$$

where $e = 1 - b^2/a^2$. With the Eq. (1), we find that the surface area of one hemisphere is 2.26×10^{10} km^2 (with an equatorial diameter of 60,268 km and a polar diameter of 54,364 km). In addition, the areas of the observational gaps are integrated over the areas of these pixels within their gaps, which yield 5.84×10^9 km^2 and 6.81×10^8 km^2 for the NH and SH, respectively. Assuming that the areas of the observational gaps have the same concentration of vortices as the observed areas shown in Fig. 1, the total numbers of vortices in these observational gaps are $9 \times 5.84 \times 10^9/2.26 \times 10^{10} \sim 2$ and $28 \times 6.81 \times 10^8/2.26 \times 10^{10} \sim 1$ for the NH and SH, respectively. The estimated numbers of vortices in the observational gaps (2 in the NH and 1 in the SH) are also used to represent the uncertainty in the total numbers of vortices. Therefore, the total numbers of vortices with uncertainties are 11 ± 2 and 29 ± 1 for the NH and SH, respectively.

Even considering uncertainties, there are significant differences in the total numbers of the vortices between the two hemispheres. Considering the two hemispheres in Fig. 1 were observed during two different time periods (2004 vs. 2008), we cannot rule out

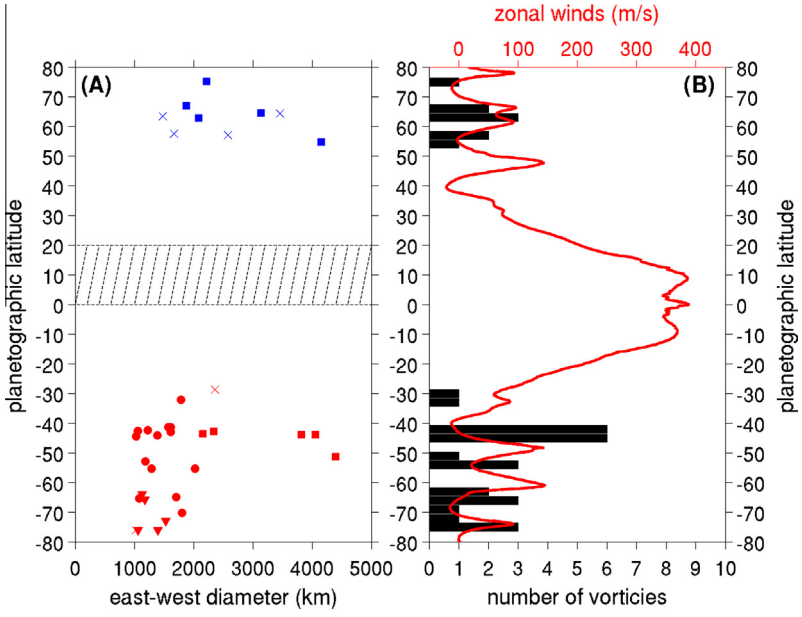

Fig. 3. Meridional distribution of vortices on Saturn in 2004/2008. (A) Vortex distribution in the plane of latitude and east–west diameter. (B) Comparison between the vortex concentration and the zonal winds. The shaded areas in panel A represent the observational gaps in the equatorial region in the NH (Fig. 1). The zonal winds in panel B come from the averaged zonal winds during a period of 2004–2009, which were measured with the CB2 images in a previous study (García-Melendo et al., 2011).

the possibility that the difference in numbers between the two hemispheres in Fig. 1 are related to the temporal variation of the total numbers of vortices in the two hemispheres (Section 3.2). However, the comparison of the numbers of vortices between the two hemispheres (Fig. 4) at the same time suggests that there are, indeed, more vortices in the SH than in the NH. This implies a trend in uneven distribution of vortices across saturnian hemispheres over time. Based on the method of estimating the vorticity of individual vortices by zonal winds introduced in Section 2, we examined the individual vorticities observed in the first global map. This method of defining vorticity is a generalized approach, so the following results may vary. In the SH in 2004, 11 of the 28 tracked vortices reveal cyclonic activity, while the remaining 17 are anti-cyclonic. In the NH, 4 of the 9 tracked vortices display cyclonic activity and the remaining 5 are anti-cyclonic.

3.2. Temporal variation of the global vortices on Saturn

To explore the temporal variation of the vortices on Saturn, we examine the public data sets on the PDS to create more global maps. Unfortunately, the observational mode after the Saturn Prime Mission (2004–2008) is not conducive to the creation of global maps. After Cassini's Prime Mission, we found only one series of images from the PDS (2009–2010) that fit the three criteria we introduced in Section 2 for creation of global maps. Fig. 4 shows the global map in the CB2 filter in 2010. Saturn was experiencing early northern spring during 2010; therefore, the equatorial and SH low latitude regions are in ring shadows.

The comparison of Figs. 4 and 1 show that there are fewer vortices in the second CB2 global map (2010) than in the first global map (2004/2008). Table 2 lists the numbers of vortices in the four categories on Saturn in 2010, which suggests that the total numbers of the vortices are 6 and 9 for the NH and the SH, respectively. Likewise, we use the ratio of the area of the observational gaps to the total area of one hemisphere to estimate the uncertainty in the total numbers of vortices in the two hemispheres. Such estimates suggest that the total numbers of vortices with the uncertainties are 7 ± 1 and 11 ± 2 for the NH and SH, respectively. Table 2 shows the variation of vortices in the four categories from the first global map and the second global map. With these uncertainties, the total numbers of vortices changed from 11 ± 2 to 7 ± 1 and from 29 ± 1 to 11 ± 2 for the NH (2008–2010) and the SH (2004–2010), respectively. The significant temporal variation in the total numbers of vortices on Saturn provides clues for the seasonal variation of the global atmosphere on Saturn. Currently, we have no concrete explanation for the physics behind the significant variation presented in this study, even though it is suggested that there are possible relationships between the global variation of vortices and the eruption of the giant storm in the end of 2010 on Saturn.

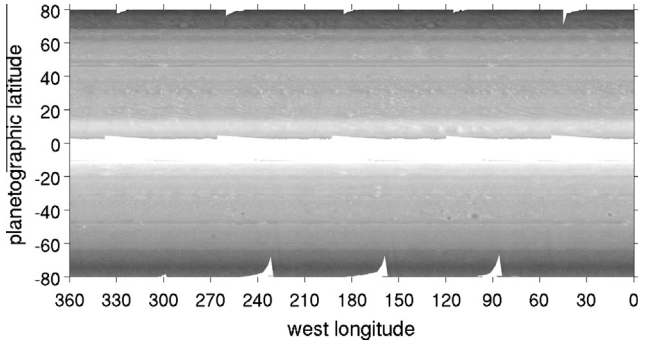

Fig. 4. Second global map of Saturn observed in the CB2 filter. The two hemispheric maps are both composed by 6 WAC images, which were observed by ISS in 2010 with a spatial resolution of ~147 km/pixel and a time separation of ~2 h. The observational gaps are shown in blank areas in the global map.

Fig. 5 shows the east–west/north–south diameter ratio of the vortices in 2010. A comparison between Fig. 2 (2004/2008) and Fig. 5 (2010) suggests that the average ratio in the SH significantly decreased from 2.19 ± 0.29 in 2004 to 1.32 ± 0.24 in 2010. In the NH, the average ratio did not significantly changed from 2008 (1.41 ± 0.23) to 2010 (1.63 ± 0.22). Fig. 6 is the meridional distribution of vortices in 2010. Panel B shows that the vortices are concentrated in the peak of westward zonal jets in the two hemispheres, consistent with the behavior of the vortex distribution in 2004/2008 (Fig. 3).

Based on the comparison of the two global maps at different times (Figs. 1 and 4) and the comparison of the analyses of vortices in the two global maps (Figs. 2 and 3 and Figs. 5 and 6), it seems that most of the vortices in the first global map (2004/2008) disappeared in the second global map (2010) by examining the locations and appearances of the vortices (size, shape, and color). The only exception is the vortex near 64°N with the east–west diameters ~3100 km (panel A in Figs. 3 and 6). This vortex in the two global maps appears nearly identical in size, shape, and location, which suggest that the two vortices are probably the same, long-lived vortex. However, we cannot rule out a possibility that the old vortex disappeared and a similar vortex appeared between 2008 and 2010 because there is no continuous observation during the period of 2008–2010.

Observed vortices also display possible variations in vorticity (cyclonic/anti-cyclonic) over time. With the method of estimating vorticity introduced in Section 2, the 2010 global map suggests that all 6 vortices in the NH are cyclonic and all 9 vortices in the SH are anti-cyclonic. The comparison between the first and second global maps suggests that anti-cyclonic vortices in the NH and the cyclonic vortices in the SH are probably instable around the observational time of the second global map (2010). Currently, we do not have a detailed explanation for the variation in the stability of vortices displayed in our global observations of Saturn.

3.3. Comparison of the global vortices between Saturn and Jupiter

Cassini not only observed Saturn, but also strategically collected data at Jupiter during its transit fly-by of the Gas Giant. The obser-

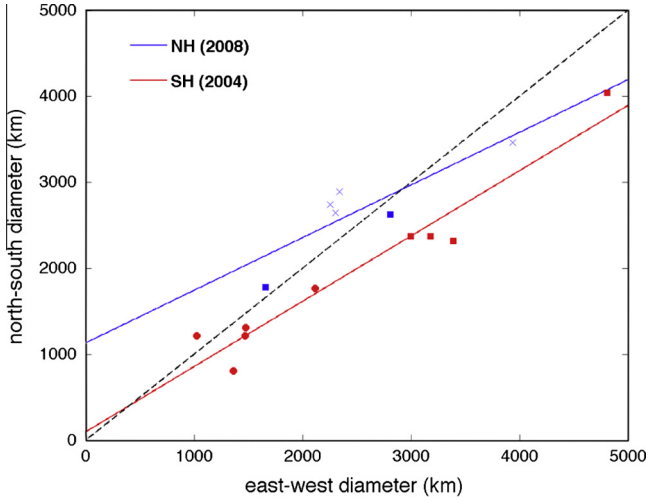

Fig. 5. Scatter plot of vortices in the two hemispheres of Saturn in 2010. Vortices are classified into the four categories shown in Fig. 7 of Vasavada et al. (2006). Circles, squares, triangles, and crosses represent category 1, 2, 3, and 4, respectively. The blue line and red line are the fitting lines for the ratios of the east–west diameters to the north–south diameters of the vortices in the NH and in the SH, respectively. The dashed black line represents the ratio as 1.0 (the east–west diameters are equal to the north–south diameters). (For interpretation of the references to color in this figure legend, the reader is referred to the web version of this article.)

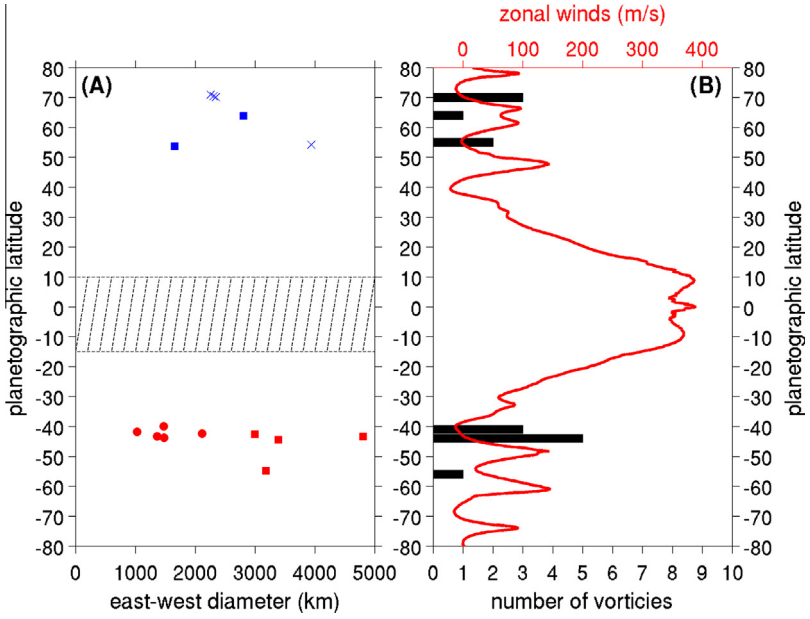

Fig. 6. Meridional distribution of vortices on Saturn in 2010. (A) Vortex distribution in the plane of latitude and east–west diameter. (B) Comparison between the vortex concentration and the zonal winds. The shaded areas in panel A represent the observational gaps in the equatorial region. The zonal winds in panel B come from the averaged zonal winds during a period of 2004–2009, which was measured with the CB2 images in a previous study (García-Melendo et al., 2011).

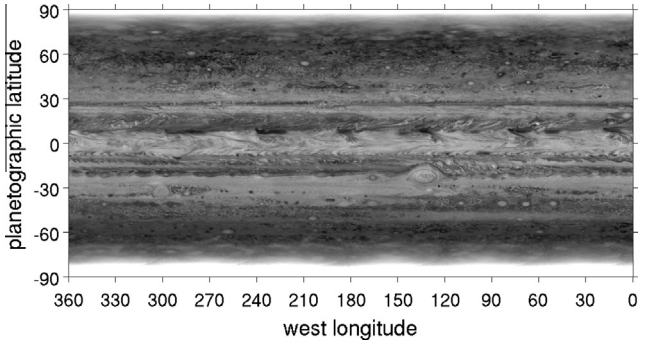

Fig. 7. Global map of Jupiter observed in the CB2 filter. The global map is composed by 7 NAC images, which were observed by ISS in 2000 with a spatial resolution of ~100 km/pixel and a time separation of ~1.5 h. The observational gaps, which are represented by the very bright areas in the polar region, are smaller in the NH than in the SH.

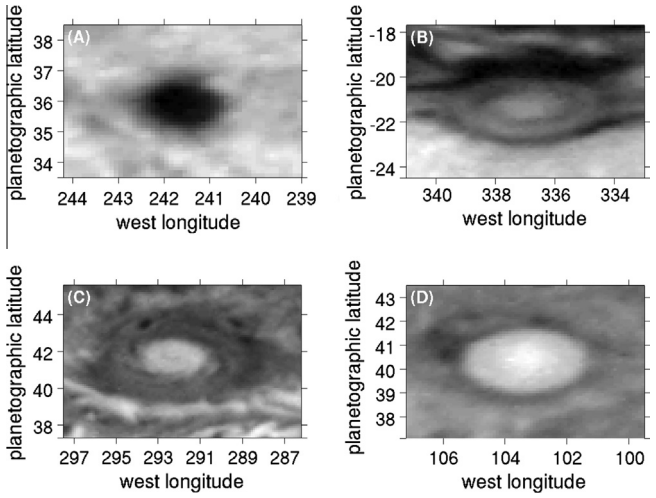

Fig. 8. Examples of four categories of vortices on Jupiter. (A) Category 1: dark. (B) Category 2: bright with a bright margin. (C) Category 3: bright centered. (D) Category 4: bright. *Note*: there are no jovian vortices belonging to category 2 on Saturn. On the contrast, there is one new category of vortices (bright with a bright margin) on Jupiter, which is defined as category 2 for Jupiter.

vations of the two giant planets by the same spacecraft provide a perfect opportunity to conduct a comparative study between them. Fig. 7 is the global map of Jupiter from the CB2 filter, taken by Cassini in 2000, which shows there are far more vortices on Jupiter than on Saturn. The vortices on Jupiter have already been explored in detail in our previous study (Li et al., 2004). In this study, we emphasize the comparison of vortices between Saturn and Jupiter.

To keep the scope of this study uniform, we only recorded those jovian vortices with east–west diameters larger than 1000 km with the global map shown in Fig. 7. In addition, we follow the categories of Fig. 7 in Vasavada et al. (2006), to organize these jovian vortices. However, there was no indication of any second-category vortices (dark with bright margin) in the global map of Jupiter shown in Fig. 7. Instead, we found a new category (bright center and circulated with bright ring) shown in panel B in Fig. 8, which were not observed in the corresponding ISS images of Saturn. We replaced the second category with the new category (bright center and circulated with bright ring) for a total of four categories of vortices on Jupiter. The Great Red Spot around 22°S and the white oval around 32°S are the two largest observed vortices, with the east–west longitude larger than 10,000 km; these unique features are not included in our analysis of jovian vortices as they are major statistical outliers.

The four categories used to classify jovian vortices are shown in Fig. 8 and the number of vortices observed in each category is shown in Table 2. Category 4 vortices (bright) are the most prevalent type observed on Jupiter. This observation is quite different from Saturn where dark vortices (category 1) dominate. Table 2 also shows there are total of 189 vortices with an uncertainty of ±2 by estimating the ratio between the area of the observational gaps and the global area. Jupiter's vortices (191 ± 2) are ~5 times and ~11 times more abundant than saturnian vortices in the first global map (40 ± 3) and the second global map (18 ± 3), respectively. Table 2 also shows that the jovian vortices are approxi-

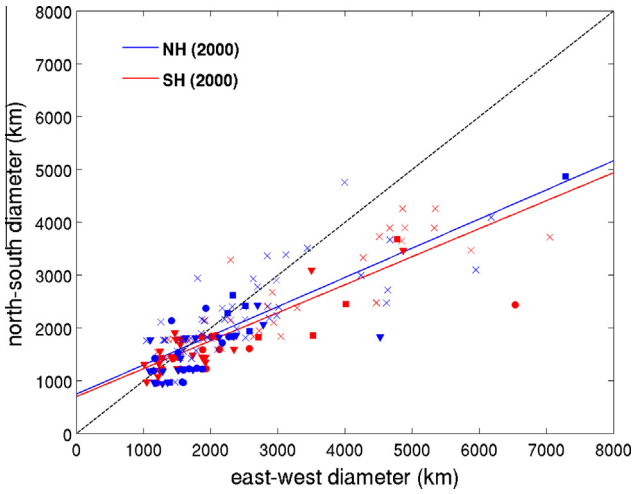

Fig. 9. Scatter plot of vortices in the two hemispheres of Jupiter in 2000. Vortices are classified into the four categories shown in Fig. 8. Circles, squares, triangles, and crosses represent category 1, 2, 3, and 4, respectively. The blue line and red line are the fitting lines for the ratios of the east–west diameters to the north–south diameters of the vortices in the NH and in the SH, respectively. The dashed black line represents the ratio as 1.0 (the east–west diameters are equal to the north–south diameters). (For interpretation of the references to color in this figure legend, the reader is referred to the web version of this article.)

mately equally distributed between the NH (99 ± 1) and SH (92 ± 1) of Jupiter. This number is starkly different from Saturn where we observe more vortices in the SH (29 ± 1 in 2004 and 11 ± 2 in 2010) than the NH (11 ± 2 in 2008 and 7 ± 1 in 2010).

We can also investigate the oblateness of jovian vortices. Fig. 9 shows the ratio of the east–west diameters to the north–south diameters and suggests that the two hemispheres have approximately the same ratios. In the NH, the ratio is larger for Jupiter (1.81 ± 0.17 in 2000) than on Saturn (1.41 ± 0.23 in 2008 and 1.63 ± 0.22 in 2010), which indicates that the vortices in the NH are more circular on Saturn than on Jupiter during this time frame. In the SH, the average ratio of vortices on Saturn changed significantly with time (Figs. 2 and 5). The average SH ratio on Jupiter (1.89 ± 0.18) is smaller than the SH ratio on Saturn in 2004 (2.19 ± 0.29) but larger than the SH ratio on Saturn in 2010 (1.32 ± 0.24). Fig. 10 shows the latitudinal distribution of the vortices on Jupiter, which are concentrated near the peak of westward zonal jets. The distribution of the relatively large vortices (>1000 km) investigated in this study is consistent with the results in the previous study (Li et al., 2004), in which the relatively small vortices are also included. The latitudinal distribution of vortices on Jupiter is also consistent with the observations of Saturn presented here (Section 3.1) and in Vasavada et al. (2006) and suggests that the atmospheric instability in these regions contributes to the generation of vortices on both giant planets (Dowling and Ingersoll, 1989; Li et al., 2004; Vasavada et al., 2006).

4. Conclusions and discussions

In this study, we processed global maps of Saturn and Jupiter from images recorded by the Cassini ISS. Based on these global maps, we conducted a global survey of Saturn's vortices with diameters larger than 1000 km. We also conducted a number of comparative studies including: the comparison of vortices between Saturn's two hemispheres, the comparison of Saturn's global vortices between different observational periods, and the comparison of the global vortices between Saturn and Jupiter.

The hemispheric comparison of vortices shows similarities (e.g., locating around the peak of westward jets) and differences (e.g., total numbers of vortices) between the two hemispheres of Saturn. The examination of the global maps at different times reveals that there was a significant decrease in the total number of vortices on Saturn from 2004/08 (40 ± 3) to 2010 (18 ± 3). The comparative study between Jupiter and Saturn shows that there are many more vortices on Jupiter (191 ± 2 in 2000) than on Saturn (40 ± 3 in 2004/08 and 18 ± 3 in 2010). The correlation between the concentrations of vortices and the peaks of the westward jets is the same between Jupiter and Saturn, suggesting that the correlation is a general phenomenon on Gas Giant Planets.

As discussed in Section 3.1, the first global map (Fig. 1 and Table 2) shows that the total number of vortices in the SH is 29 ± 1 in 2004. This is more than two times the total number of vortices 11 ± 2 in the NH in 2008, presenting an uneven distribu-

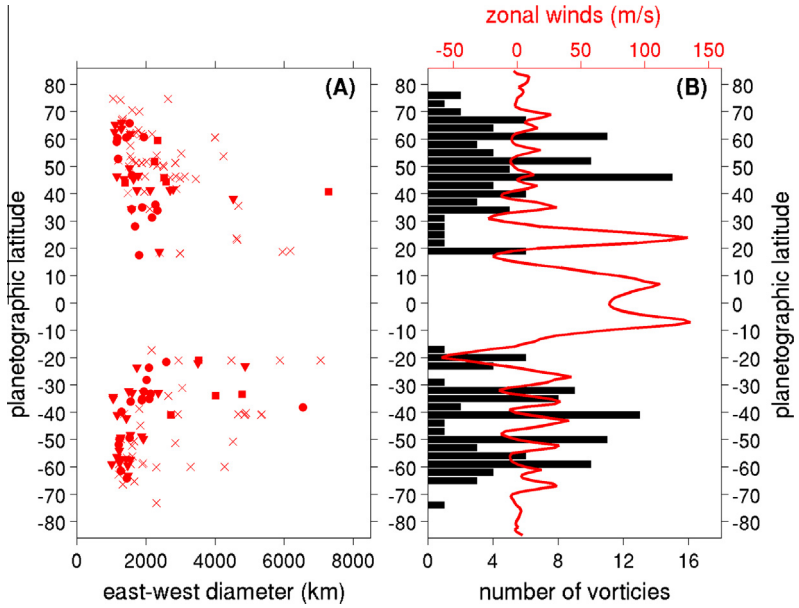

Fig. 10. Meridional distribution of vortices on Jupiter in 2000. (A) Vortex distribution in the plane of latitude and east–west diameter. (B) Comparison between the vortex concentration and the zonal winds. The zonal winds in panel B (red line) comes from a previous study (Porco et al., 2003). (For interpretation of the references to color in this figure legend, the reader is referred to the web version of this article.)

tion between hemispheres. Furthering the study, simultaneous observations of the two hemispheres (Fig. 4) shows that the total number of vortices is more than 1.5 times greater in the SH (11 ± 2) than in the NH (7 ± 1) in 2010. Therefore, it is observed that there are significantly more vortices in the SH than in the NH on Saturn during the period of 2004–2010. On the other hand, Jupiter displays the quasi-equal distribution of vortices between the two hemispheres, which is most likely related to the small obliquity (3.1°) and hence relatively small seasonal variation. Unlike Jupiter, Saturn has a relatively large seasonal solar insolation variation due to its large obliquity (26.7°). However, it seems that the seasonal cycle is not the only factor contributing to the different numbers of vortices between the two hemispheres on Saturn. The first global map (2004/2008, before the northern spring equinox) and the second global map (2010, after the northern spring equinox) both suggest there are more vortices in the SH than in the NH. Saturn's upper troposphere, where the vortices are located, has a long radiative time constant equal to ~24 Earth years (Conrath et al., 1989). The long radiative time constant results in a time lag in the response of the atmospheric thermal structure to the varying solar radiance due to the seasonal change on Saturn (Li et al., 2010). The time lag in the response of thermal structure and the related dynamical processes in Saturn's atmosphere also helps explain the fact that there are more vortices in the SH than in the NH even though Saturn's season changed from the northern winter (2004/2008) to the northern spring (2010).

The other factor affecting the number of vortices on Saturn is the interaction between the vortices and large-scale atmospheric processes. The comparison of two global maps at different times (Section 3.2) suggests that the total number of the global vortices changed from 40 ± 3 to 18 ± 3 during the period of 2004–2010. The time of the second global map (September, 2010) is about 3 months before the eruption of the giant storm on Saturn (December, 2010) (Sanchez-Lavega et al., 2011; Fischer et al., 2011; Fletcher et al., 2011). A previous study (Marcus, 2004) suggested that there are some relationships between the vortex dynamics and the global-scale thermal structure on Jupiter, in which a decrease of the total number of vortices will significantly modify Jupiter's global thermal structure by 10 K. It is possible that the global variation of vortices and the related modifications in the large-scale thermal structure play some roles in the eruption and development of the 2010 giant storm on Saturn, but some theoretical studies are needed to illuminate such a relationship. On the other hand, the development of the 2010 giant storm unquestionably affected NH vortex activities on Saturn, as suggested by some previous studies (Fletcher et al., 2012; Sayanagi et al., 2013). Analyzing more public Cassini data sets that are becoming available, future studies will include tracking the temporal variation of global vortices after the 2010 giant storm. Subsequent analysis will shed more light on the interaction between the global vortices and the giant storm on Saturn.

Acknowledgments

NASA Cassini Data Analysis and Outer Planets Research Programs funded this work. We also acknowledge the Cassini ISS team for providing the multi-filter images of Jupiter and Saturn. S.M.H. is supported by NSF Astronomy and Astrophysics Postdoctoral Fellowship AST-1102827.

References

Bevington, P.R., Robinson, D.K., 2003. Data Reduction and Error Analysis for the Physical Sciences, third ed. McGraw-Hill, New York.
Conrath, B.J., Hanel, R.A., Samuelson, R.E., 1989. Thermal structure and heat balance of the outer planets. In: Atreya, S.K., Pollack, J.B., Matthews, M.S. (Eds.), Origin and Evolution of Planetary and Satellite Atmospheres. The University of Arizona Press, Arizona.
Coxeter, H.S.M., 1989. Introduction to Geometry, second ed. John Willey & Sons, Hoboken, New Jersey.
Del Genio, A.D., Barbara, J.M., Ferrier, J., Ingersoll, A.P., West, R.A., Vasavada, A.R., Spitale, J., Porco, C.C., 2007. Saturn eddy momentum fluxes and convection: First estimates from Cassini images. Icarus 189, 479–492.
Del Genio, A.D. et al., 2009. Saturn atmospheric structure and dynamics. In: Dougherty, M.K., Esposito, L.W., Krimigis, S.M. (Eds.), Saturn from Cassini–Huygens. Springer, pp. 113–159.
del Rio-Gaztelurrutia, T., Legarreta, J., Hueso, R., Perez-Hoyos, S., Sanchez-Lavega, A., 2010. A long-lived cyclone in Saturn's atmosphere: Observations and models. Icarus 209 (2), 665–681. http://dx.doi.org/10.1016/j.icarus.2010.04.002.
Dowling, T.E., Ingersoll, A.P., 1989. Jupiter's Great Red Spot as a shallow water system. J. Atmos. Sci. 46, 3256–3278.
Fischer, G. et al., 2011. A giant thunderstorm on Saturn. Nature 475, 75–77.
Fletcher, L.N. et al., 2011. Thermal structure and dynamics of Saturn's northern springtime disturbance. Science 332, 1413–1417.
Fletcher, L.N. et al., 2012. The origin and evolution of Saturn's 2011–2012 stratospheric vortex. Icarus 221, 560–586.
García-Melendo et al., 2011. Saturn's zonal wind profile in 2004–2009 from Cassini ISS images and its long-term variability. Icarus 215, 62–74.
Ingersoll, A.P., Cuong, P.-G., 1981. Numerical model of long-lived jovian vortices. J. Atmos. Sci. 38, 2067–2074.
Ingersoll, A.P., Beebe, R.F., Mitchell, J.L., Garneau, G.W., Yagi, G.M., Shu, F.H., 1981. Interaction of eddies and zonal flow on Jupiter as inferred from Voyager 1 and 2 images. J. Geophys. Res. 86, 8733–8743.
Ingersoll, A.P. et al., 2004. Dynamics of Jupiter's atmosphere. In: Bagenal, F., Dowling, T.E., McKinnon, W.B. (Eds.), Jupiter: The Planet, Satellites, and Magnetosphere. Cambridge Univ. Press, Cambridge.
Li, L., Ingersoll, A.P., Vasavada, A.R., Porco, C.C., Del Genio, A.D., Ewald, S.P., 2004. Life cycles of spots on Jupiter from Cassini images. Icarus 172 (1), 9–23.
Li, L., Ingersoll, A.P., Huang, X.L., 2006a. Interaction of moist convection with zonal jets on Jupiter and Saturn. Icarus 180, 113–123.
Li, L., Ingersoll, A.P., Vasavada, A.R., Simon-Miller, A.A., Achterberg, R.K., Ewald, S.P., Dyudina, U.A., Porco, C.C., West, R.A., Flasar, F.M., 2006b. Waves in Jupiter's atmosphere observed by the Cassini ISS and CIRS instruments. Icarus 185, 416–419.
Li, L. et al., 2010. Emitted power of Saturn. J. Geophys. Res. – Planets 115. Art. No. E11002.
Mac Low, M.-M., Ingersoll, A.P., 1986. Merging of vortices in the atmosphere of Jupiter: An analysis of Voyager images. Icarus 65, 353–369.
Marcus, P.S., Kundu, T., Lee, C., 2000. Vortex dynamics and zonal flows. Phys. Plasmas 7, 1630–1640.
Marcus, P.S., 2004. Prediction of a global climate change on Jupiter. Nature 428, 828–831.
Minnaert, M., 1941. The reciprocity principle in lunar photometry. Astrophys. J. 93, 403–410.
Morales-Juberias, R., Sanchez-Lavega, A., Lecacheux, J., Colas, F., 2002. A comparative study of jovian anticyclone properties from a six-year (1994–2000) survey. Icarus 157, 76–90.
Perez-Hoyos, S., Sanchez-Lavega, A., 2006. On the vertical wind shear of Saturn's equatorial jet at cloud level. Icarus 180, 161–175.
Porco, C. et al., 2003. Cassini imaging of Jupiter's atmosphere, satellites, and rings. Science 299 (5612), 1541–1547. http://dx.doi.org/10.1126/science.1079462.
Porco, C.C. et al., 2004. Cassini imaging science: Instrument characteristics and anticipated scientific investigations at Saturn. Space Sci. Rev. 115, 363–497.
Salyk, C., Ingersoll, A.P., Lorre, J., Vasavada, A.R., Ewald, S., Del Genio, A.D., 2006. Interaction between eddies and mean flow in Jupiter's atmosphere: Analysis of Cassini imaging data. Icarus 185, 430–442.
Sánchez-Lavega, A., Hueso, R., Perez-Hoyos, S., Rojas, J.F., French, R.G., 2004. Saturn's cloud morphology and zonal winds before the Cassini encounter. Icarus 170, 519–523.
Sanchez-Lavega, A., Hueso, R., Perez-Hoyos, S., 2007. The three-dimensional structure of Saturn's equatorial jet at cloud level. Icarus 187, 510–519.
Sanchez-Lavega, A. et al., 2011. Deep winds beneath Saturn's upper clouds from a seasonal long-lived planetary-scale storm. Nature 475, 71–74.
Sayanagi, K.M. et al., 2013. Dynamics of Saturn's great storm of 2010–2011 from Cassini ISS and RPWS. Icarus 223, 460–478.
Showman, A.P., 2007. Numerical simulations of forced shallow-water turbulence: Effects of moist convection on the large-scale circulation of Jupiter and Saturn. J. Atmos. Sci. 64, 3132–3157.
Smith et al., 1981. Encounter with Saturn: Voyager 1 imaging science results. Science 212, 163–191.
Smith et al., 1982. A new look at the Saturn system: The Voyager 2 images. Science 215, 504–537.
Sromovsky, L.A., Revercomb, H.E., Krauss, R.J., Suomi, V.E., 1983. Voyager 2 observations of Saturn's northern mid-latitude cloud features: Morphology, motions, and evolution. J. Geophys. Res. 88 (A11), 8650–8666.
Vasavada, A.R., Showman, A.P., 2005. Jovian atmospheric dynamics: An update after Galileo and Cassini. Rep. Prog. Phys. 68, 1935–1996.
Vasavada, A.R. et al., 2006. Cassini imaging of Saturn: Southern Hemisphere winds and vortices. J. Geophys. Res. 111, E05004. http://dx.doi.org/10.1029/2005JE002563.
Williams, G.P., Yamagata, T., 1984. Geostrophic regimes, intermediate solitary vortices and jovian eddies. J. Atmos. Sci. 41, 453–478.